

# NUMERICAL CONSIDERATIONS FOR THREE-DIMENSIONAL SOUND PROPAGATION MODELING: COORDINATE SYSTEMS AND GRID SIZES

YING-TSONG LIN<sup>1</sup>  
ARTHUR E. NEWHALL<sup>1</sup>  
TIMOTHY F. DUDA<sup>1</sup>  
CHI-FANG CHEN<sup>2</sup>

<sup>1</sup>*Woods Hole Oceanographic Institution  
WHOI AOPPE Dept. MS 11  
Woods Hole, Massachusetts 02543  
United States of America  
email: ytlin@whoi.edu, anewhall@whoi.edu, tduda@whoi.edu*

<sup>2</sup>*National Taiwan University  
Department of Engineering Science and Ocean Engineering  
No. 1, Sec. 4, Roosevelt Road, Taipei, 10617  
Taiwan  
email: chifang@ntu.edu.tw*

*Three-dimensional sound propagation models with a parabolic approximate wave equation (PE) solved in either Cartesian  $(x,y,z)$  or cylindrical  $(r,\theta,z)$  coordinate systems are compared. The Split-step Fourier marching algorithm is employed. The solutions can be made arbitrarily more accurate by increasing grid resolution. Both models have limited valid area in horizontal azimuth with respect to the marching direction, which is radial for the cylindrical model and is along the  $x$  axis for the Cartesian model. Selection between these two models for a given problem depends on the type of sound wave field. For a cylindrical wave-like field the cylindrical model is more suitable; on the other hand, for a plane wave-like field the Cartesian model is advantageous. In terms of numerical implementation, the cylindrical model requires entry or calculation of the free-space propagator at each step, while this numerical item is spatially uniform for the Cartesian method thus reducing computation time. Conventional implementation of three-dimensional PE models in a cylindrical coordinate system with fixed azimuth grids suffers from loss of resolution in far field, and a method of re-sampling azimuth grids is proposed in this paper to overcome this defect. Further analysis of errors for specific frequencies and grid sizes applicable to ocean acoustics problems will be given in the presentation.*

## 1. Introduction

Two numerical considerations for three-dimensional (3D) sound propagation modeling with a wide angle parabolic-equation (PE) approximation are discussed in this paper. These

are the coordinate system used in the model, and the grid size of environmental sampling. Cylindrical and Cartesian coordinate systems are considered, and the same PE approximation with the Split-step Fourier algorithm [1] is used in each for consistent comparisons. Mathematical analysis is performed to study the limitation of the PE models using different coordinate systems and to quantify the required grid sizes. Calculation results for two idealized problems simulating conditions of shelfbreaks and submarine seamounts are also presented.

The idealized seamount in the first problem is considered to be axial-symmetric. Thus, if the source is placed right above the seamount tip, the sound field is independent to the azimuth, termed Nx2D/azimuthal-2D. This provides a good benchmark to test the 3D Cartesian PE, whose coordinate system is not effective to describe the bathymetry. The source is also placed away from the tip, and provide a scenario to test the 3D cylindrical PE for the issue of irregular resolution (further and further away from the PE origin, the azimuth sector is getting bigger and bigger). A method of re-sampling model grids is proposed for implementing 3D cylindrical PE, and the conventional defect of irregular resolution may be overcome, as shown in this paper. The second proposed problem is a classic benchmark, a slope/wedge problem, for 3D sound propagation models. In solving this problem, two different PE marching directions, down slope and across slope will be chosen for the 3D Cartesian PE. With the first marching direction (down slope), no transversal step-wise approximation is imposed, but the step-wise approximation is applied in the marching direction. The situation is opposite with the second marching direction (across slope), presented in this paper. The calculation results from the cylindrical PE model are also compared in this benchmark problem.

In addition to the mathematical analysis of model grid sizes, a convergent test on solving the proposed problems will be presented in the talk. The current consider is on discretizing the bathymetry. The grid size issue for sampling water column is beyond the scope of this paper and thus is deferred to the future.

## 2. Split-step Fourier 3D PE

Two different implementations of the Split-step Fourier 3D PE are considered here. The difference is on the use of coordinate systems; one is using the Cartesian coordinate system and another is using the cylindrical coordinate system.

### 2a. Theory

The parabolic wave equation which incorporates an assumption of one-way propagation can be generally written in either Cartesian  $(x, y, z)$  or cylindrical  $(r, \theta, z)$  coordinate in the following two ways:

$$\frac{\partial}{\partial x} \varphi(x, y, z) = ik_0 \left\{ \sqrt{n^2(x, y, z) + k_0^{-2} \left( \frac{\partial^2}{\partial y^2} + \frac{\partial^2}{\partial z^2} \right)} - 1 \right\} \varphi(x, y, z), \quad (1.1)$$

$$\frac{\partial}{\partial r} \varphi(r, \theta, z) = ik_0 \left\{ \sqrt{n^2(r, \theta, z) + k_0^{-2} \left( \frac{1}{r^2} \frac{\partial^2}{\partial \theta^2} + \frac{\partial^2}{\partial z^2} \right)} - 1 \right\} \varphi(r, \theta, z), \quad (1.2)$$

Here,  $n = k/k_0$  is the refraction index,  $k = \omega/c$  is the local wavenumber at frequency  $\omega$  for wave speed  $c$ , and  $k_0$  is a reference wavenumber. The derivations of these two approximate wave equations differ only slightly. The Cartesian PE originates from decomposing the exact forward 3D pressure ( $p$ ) into  $p(x, y, z) = \varphi(x, y, z) \exp(ik_0 r)$ . The cylindrical PE originates from  $p(r, \theta, z) = r^{-1/2} \varphi(r, \theta, z) \exp(ik_0 r)$  with a far-field approximation. The equations have a nearly identical form in both Cartesian and cylindrical coordinates, the difference being the scaling factor  $1/r$  within the second derivative operator. A unified notation for this second derivative operator can be defined below.

$$\begin{cases} \nabla_V^2 = \frac{\partial^2}{\partial y^2} + \frac{\partial^2}{\partial z^2} & \text{in } (x, y, z) \text{ coordinate} \\ \nabla_V^2 = \frac{1}{r^2} \frac{\partial^2}{\partial \theta^2} + \frac{\partial^2}{\partial z^2} & \text{in } (r, \theta, z) \text{ coordiante} \end{cases} \quad (2)$$

A radical approximation to a square-root operator proposed by Feit and Flect [2] is considered here:

$$\sqrt{n^2 + k_0^{-2} \nabla_V^2} \cong \sqrt{1 + k_0^{-2} \nabla_V^2} + n - 1. \quad (3)$$

This radical approximation recovers the original square-root operator when  $n=1$ . This approximation was in fact used by Thomson and Chapman [3], leading to a wide angle 2D PE. The 3D PE theory presented here can be considered equivalent to Thomson and Chapman's 2D PE. Implementation of the 3D version with a Cartesian coordinate system is analyzed in Huang and Fehler [4] for seismologic applications and in Duda [5] for underwater acoustic applications. The formal finite difference solution of Eq. (1) with this radical approximation can be found as:

$$\tilde{\varphi}(\eta + \Delta\eta) = \exp \left\{ i\Delta\eta \left( \sqrt{k_0^2 + \nabla_V^2} + k - 2k_0 \right) \right\} \tilde{\varphi}(\eta), \quad (4)$$

where the dependence on the other two spatial variables ( $y, z$ ) or ( $\theta, z$ ) is not indicated, for conciseness. The tilde indicates the solution is an approximate solution. The marching coordinate  $\eta$  is either  $r$  or  $x$ . The exponential operator can be separated according to the split-step algorithm [1-6], and the following split-step solution has a second-order accuracy with respect to  $\Delta r$ , i.e.,  $O(\Delta r^2)$ :

$$\begin{aligned} & \exp \left\{ -i \frac{\Delta\eta}{2} \mathbf{B}(\eta + \Delta\eta) \right\} \exp \left\{ -i \frac{\Delta\eta}{2} \mathbf{A}(\eta + \Delta\eta) \right\} \tilde{\varphi}(\eta + \Delta\eta) \\ &= \exp \left\{ i \frac{\Delta\eta}{2} \mathbf{B}(\eta) \right\} \exp \left\{ i \frac{\Delta\eta}{2} \mathbf{A}(\eta) \right\} \tilde{\varphi}(\eta), \end{aligned} \quad (5)$$

where operator  $\mathbf{A}$  denotes  $(\sqrt{k_0^2 + \nabla_V^2} - k_0)$ , operator  $\mathbf{B}$  denotes  $(k - k_0)$ , and the range-dependency of both operators are also noted. To solve the split-step solution numerically, one can employ the Fourier transform and combine the  $\mathbf{A}$  and  $\mathbf{B}$  operators, leading to

$$\mathcal{F}^{-1} \{ \mathbf{Q}^{-1}(\eta + \Delta\eta) \tilde{\Phi}(\eta + \Delta\eta) \} = \exp \left( i\Delta\eta \mathbf{B} \left( \eta + \frac{\Delta\eta}{2} \right) \right) \mathcal{F}^{-1} \{ \mathbf{Q}(\eta) \tilde{\Phi}(\eta) \}, \quad (6.1)$$

which can also be written as

$$\tilde{\Phi}(\eta + \Delta\eta) = \mathbf{Q}(\eta + \Delta\eta) \mathcal{F} \left\{ \exp \left( i \Delta\eta \mathbf{B} \left( \eta + \frac{\Delta\eta}{2} \right) \right) \mathcal{F}^{-1} \{ \mathbf{Q}(\eta) \tilde{\Phi}(\eta) \} \right\} \quad (6.2)$$

Here,  $\mathcal{F}$  indicates Fourier transform,  $\tilde{\Phi}$  is the wavenumber spectrum of  $\tilde{\varphi}$ , i.e.,  $\mathcal{F}\{\tilde{\varphi}\}$ , and the average of  $\mathbf{B}$  at ranges  $\eta$  and  $\eta + \Delta\eta$  has been approximated to  $\mathbf{B}(\eta + \Delta\eta/2)$ .  $\mathbf{Q}(\eta)$  in the equation denotes a wavenumber-dependent free-domain (straight line) propagation from  $\eta$  to  $\eta + \Delta\eta/2$ , applied in the wavenumber domain, with the given reference wavenumber  $k_0$ :

$$\mathbf{Q}(\eta) = \exp \left\{ i \frac{\Delta\eta}{2} \left( \sqrt{k_0^2 - k_{\mathbf{V}}^2} - k_0 \right) \right\}, \quad (7)$$

where  $k_{\mathbf{V}} = (r^{-2}k_{\theta}^2 + k_z^2)^{1/2}$  in cylindrical PE ( $\eta = r$  also), indicating a vertical wavenumber in the  $\theta$ - $z$  plane, and where  $k_{\mathbf{V}} = (k_y^2 + k_z^2)^{1/2}$  in Cartesian PE. The 2D Fourier transform pairs used here are provided below, separately for both Cartesian and cylindrical PE's.

$$\begin{cases} F(k_y, k_z) = \int_{\mathbb{R}^2} f(y, z) e^{-i(k_y y + k_z z)} dy dz \\ f(y, z) = \frac{1}{(2\pi)^2} \int_{\mathbb{R}^2} F(k_y, k_z) e^{i(k_y y + k_z z)} dk_y dk_z \end{cases} \quad (8.1)$$

$$\begin{cases} F(k_{\theta}, k_z) = \int_{\mathbb{R}^2} f(\theta, z) e^{-i(k_{\theta} \theta + k_z z)} r d\theta dz \\ f(\theta, z) = \frac{1}{(2\pi)^2} \int_{\mathbb{R}^2} F(k_{\theta}, k_z) e^{i(k_{\theta} \theta + k_z z)} r^{-1} dk_{\theta} dk_z \end{cases} \quad (8.2)$$

Note that if both forward and inverse Fourier transforms are operated at the same radial distance in the cylindrical coordinate system, such as Eq. (6.1), the length scales  $r$  and  $r^{-1}$  in the transform cancel out.

## 2b. Error analysis of PE approximation

One can take a normal mode approach proposed by McDaniel [7] to analyze the phase errors of any rational linear PE approximations; however, McDaniel's normal mode analysis cannot be applied to a radical PE approximation.

To assess the accuracy of radical approximation Eq. (3), we can analyze the error bound of an approximation error defined as  $\mathbf{E} = \left( \sqrt{1 + k_0^{-2} \nabla_{\mathbf{V}}^2} + n - 1 \right)^2 - (n^2 + k_0^{-2} \nabla_{\mathbf{V}}^2)$ . This error analysis was in fact proposed by Feit and Flect [2] and used by Thomson and Chapman [3]. For a single wavenumber component of the 3D sound field  $\exp[i(k_x x + k_y y + k_z z)]$ , the length of  $\nabla_{\mathbf{V}}^2 \varphi$  is  $\sin^2 \zeta$ , where  $\zeta$  is an angle with respect to the  $x$  axis. This is also true for cylindrical PE when considering only  $\varphi(r, \theta, z) = \exp[i(k_r r + k_{\theta} \theta + k_z z) - ik_0 x]$  and  $\zeta$  being with respect to the radial axis. The error bound for the radical approximation to the single wavenumber component is shown to be [3]

$$|\mathbf{E}(\delta n, \zeta)| \leq 2|\delta n| |\cos \zeta - 1|, \quad (9)$$

where  $\delta n$  is the anomaly of the refraction index, i.e.,  $n = 1 + \delta n$ . For a comparison, the error bound of Tappert's standard PE [1], where  $\sqrt{n^2 + k_0^{-2} \nabla_V^2} \cong (1 + n^2 + k_0^{-2} \nabla_V^2)/2$ , can be found to be  $[|\delta n|(2 + |\delta n|) + \sin^2 \zeta]^2/4$ , and Fig. 1 shows the error bounds for both approximations as a function of  $\zeta$  and  $\delta n$ . A straightforward comparison shows that Feit and Flect's approximation achieves better accuracy. In other words, a PE model with the radical approximation to the square-root operator can in general achieve better accuracy in wider propagation angles with respect to PE marching direction.

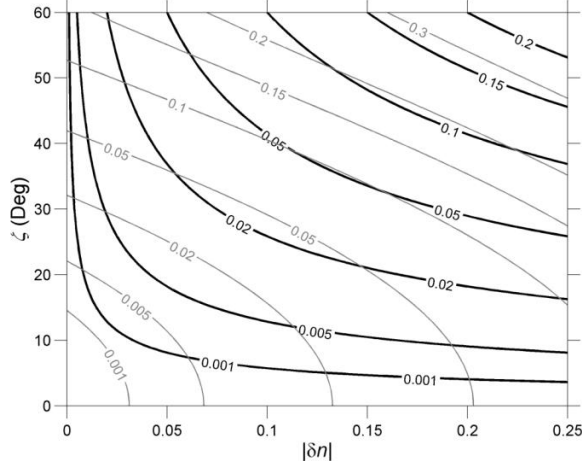


FIG. 1: Comparison of the accuracy of two different PE propagation approximations. The dark contours are the error bounds of using Feit and Flect's radical approximation, Eq.(3), and the light contours are the error bounds of Tappert's standard rational approximation.

### 2c. Differences between Cartesian and cylindrical PE's

From the error analysis presented above, one can see that the PE approximation in either Cartesian or cylindrical coordinate has the same valid angle range with respect to their own marching direction,  $\hat{e}_x$  and  $\hat{e}_r$ , respectively. But, because the direction of the radial unit vector  $\hat{e}_r$  varies azimuthally, it makes analyses of cylindrical-wave type fields easier with cylindrical PE; however, this azimuthal variation is not necessary for analyzing plane-wave type fields, where Cartesian PE is more suitable.

In terms of numerical implementations (details are provided in the following section), cylindrical PE often suffers from losing its resolution in horizontal at long ranges, and it requires recalculation of the free propagator Eq. (7) at each marching step because of its range dependency. A marching algorithm with re-sampled grids is provided later in this paper to achieve non-degraded resolution. This attempt is to provide a better numerical model when it is necessary to use cylindrical PE. Depending on the nature of the analyzed sound field, Cartesian PE might still be superior than the improved cylindrical PE.

## 3. Numerical implementation

### 3a. Discrete Fourier transform

Implementation of split-step Fourier PE, Eq.(6), requires numerical computations of Fourier transform, and from the sampling theory the discrete spatial and wavenumber domains are connected in the following way.

$$\begin{cases} k_{y \max} = \pi/\Delta y, \Delta k_y = \pi/L_y \quad (|y| \leq L_y, |k_y| \leq k_{y \max}) \\ k_{z \max} = \pi/\Delta z, \Delta k_z = \pi/L_z \quad (|z| \leq L_z, |k_z| \leq k_{z \max}) \\ k_{\theta \max} = \pi/\Delta \theta, \Delta k_\theta = \pi/L_\theta \quad (|\theta| \leq L_\theta, |k_\theta| \leq k_{\theta \max}) \end{cases} \quad (10)$$

These relations are fundamental, and they actually govern the requirements for the model grid size. Consider that the goal of sound propagation modeling is to resolve all of the arrivals less than a given arrival angle  $|\zeta| \leq \zeta_{\max}$  with a minimal required angular resolution  $\Delta\zeta_{\min}$ . Note again that the arrival angle  $\zeta$  is with respect to the PE marching direction, i.e.,  $\hat{e}_x$  in Cartesian coordinate and  $\hat{e}_r$  in cylindrical coordinate. With the sampling theory, one can determine the required  $\Delta k_{y,z,\theta}$  and  $k_{y,z,\theta \max}$  from the geometric relation of wavenumber components, i.e.,  $(k_y^2 + k_z^2)^{1/2} = |\vec{k}| \sin \zeta$  and  $(k_\theta^2/r^2 + k_z^2)^{1/2} = |\vec{k}| \sin \zeta$ . The details are provided below.

The free-domain propagation step in the Split-step Fourier PE is as though sound propagates in the field with a constant media wavenumber  $k_0$ . In order to resolve all of the arrivals less than a given angle  $\zeta_{\max}$ ,  $k_{y,z,\theta \max}$  must meet the following condition:

$$k_{y,z \max} \geq k_0 \sin \zeta_{\max} \quad \text{and} \quad k_{\theta \max} \geq k_0 r \sin \zeta_{\max} , \quad (11.1)$$

or equivalently for  $\Delta y$ ,  $\Delta z$  and  $\Delta \theta$ ,

$$\Delta y, \Delta z \leq (\sin \zeta_{\max})^{-1} \lambda_0/2 \quad \text{and} \quad \Delta \theta \leq (r \sin \zeta_{\max})^{-1} \lambda_0/2 . \quad (11.2)$$

It can be also shown that the interval between resolved arrival angles in a discrete Fourier model  $\Delta\zeta$  equals to  $k_0^{-1} \sec \zeta \Delta k_{y,z}$  in Cartesian coordinate, or  $r^{-1}(k_0^{-1} \sec \zeta \Delta k_\theta - \tan \zeta \Delta r)$  in cylindrical coordinate. Therefore, to achieve a given angular resolution  $\Delta\zeta_{\min}$ ,  $\Delta k_{y,z,\theta}$  has to satisfy the next condition:

$$\Delta k_{y,z} \leq k_0 \cos \zeta \Delta\zeta_{\min} \quad \text{and} \quad \Delta k_\theta \leq k_0 (r \cos \zeta \Delta\zeta_{\min} + \sin \zeta \Delta r) , \quad (12.1)$$

or equivalently for  $L_y$ ,  $L_z$  and  $L_\theta$ ,

$$L_{y,z} \geq (\cos \zeta \Delta\zeta_{\min})^{-1} \lambda_0/2 \quad \text{and} \quad L_\theta \geq (r \cos \zeta \Delta\zeta_{\min} + \sin \zeta \Delta r)^{-1} \lambda_0/2 . \quad (12.2)$$

Examination of these conditions reveals that the required  $\Delta\theta$  changes with the radial distance, as well as the required angular aperture  $L_\theta$ . For a conventional marching algorithm used in cylindrical PE's, i.e., marching along each radial, thus fixed  $\Delta\theta$ , the maximal arrival angle that the PE model can resolve is always smaller at larger ranges comparing to the value at shorter ranges. This will cause a numerical problem, because to a certain distance a fixed- $\Delta\theta$  PE will lose its ability to resolve horizontal refraction in a 3D field. One simple way to fix the problem is to make  $\Delta\theta$  very small, but this results in unnecessary oversampling at short ranges and wasting computation resources.

### **3b. Model grid and marching algorithm**

Implementing a PE model in Cartesian coordinate is less troublesome than implementing it in cylindrical coordinate. Since the Cartesian grid is uniform everywhere, we just need a fixed grid on  $(y, z)$  and march the solutions along  $x$ . A marching algorithm with re-sampled

azimuth grid is provided here for using cylindrical PE. In brief, this method is to fix the angular aperture  $L_\theta$  but reduce the azimuth grid interval  $\Delta\theta$  in radial to satisfy the sampling condition, Eq. (12).

The original PE marching algorithm uses a fixed  $\theta$  grid so that the solution at a range  $r$ ,  $\tilde{\varphi}(r, \theta_j, z_k)$ , can be marched to the next range  $\tilde{\varphi}(r + \Delta r, \theta_j, z_k)$  seamlessly on  $(\theta_j, z_k)$ . The same concept also applies if we consider marching in wavenumber domain; in other words, with a fixed wavenumber grid we can march  $\tilde{\Phi}(r, k_{\theta_j}, k_{z_k})$  to  $\tilde{\Phi}(r + \Delta r, k_{\theta_j}, k_{z_k})$ . The concept of marching wavenumber spectrum appears advantageous when we consider the maximal wavenumber required for resolving a given arrival angle, i.e., Eq.(12.1). Since the required maximal wavenumber at a shorter range is smaller than the value at a longer range, the initial wavenumber aperture can be smaller. When a larger aperture is required, we can zero-pad the spectrum at both ends with the same  $\Delta k_\theta$  and continue the marching procedure. This zero-padding technique may still have the problem of tracking arrivals that go over the angular aperture, and a simple solution is to make  $\Delta k_\theta$  smaller (i.e., with a larger angular aperture) to capture more arrival angles. Further investigation is required to solve this problem.

The zero-padding of wavenumber spectrum can be done at each range, or intermittently when a larger wavenumber aperture is required. For the intermittent approach, it is recommended to double the aperture, which results in reducing  $\Delta\theta$  by a half. Effectively, this is a spatial upsampling by a factor of two, and it can be regarded as a standard upsampling procedure used in digital signal processing [8].

#### 4. Numerical examples

This section briefs two numerical examples showing agreements of the 3D PE models presented above. A complete model comparisons will be given in the talk.

The water sound speed in the examples is a constant of 1500 m/s, and the bottom is homogeneous with 1650 m/s sound speed,  $1.5 \text{ km/m}^3$  density and 0.5 dB-per-wavelength attenuation. The modeled sound source is placed at the origin of horizontal coordinates and 250 m in depth. The sound source transmits continuous sinusoidal wave of 100 Hz. The modeling results of a idealized slope/wedge problem are shown in Fig. 2, and the ones of another idealized seamount problem are shown in Fig. 3. The model grid size is 6 m in marching direction, 1 m in depth and 2.5 m in horizontal. Note that the azimuth grid re-sampling described in the previous section is applied to the cylindrical PE model, and once the azimuth grid size is over 2.5 m the angular interval  $\Delta\theta$  is reduced by a half.

In the first example, the wedge has a slope of  $12.68^\circ$ , and the water depth is 100 m at the shallow part and 1000 m at the deep part, as shown in Fig. 2a. Comparing the solutions on the vertical slice along the slope at  $Y = 0$  (Fig. 2b-2d) reveals that the Nx2D model does not agree with the 3D models. It is not surprised because there is a significant 3D effect (more precisely, horizontal refraction) caused by the sloping bottom. It is worth noting that the 3D solutions on the vertical slice, shown in Fig. 2c and 2d, reach an excellent agreement. The 3D solutions on a horizontal plane at the source depth are also shown in Fig. 2e and 2f. Comparing the interference patterns from both models, it is found that at a wider azimuth angle the Cartesian PE no longer produces valid solutions, as being pointed out in the error analysis section 2b. Nevertheless, within its valid azimuth range the Cartesian PE does produce solutions agreeing with the cylindrical PE, which computation time is in general many times slower.

In the second example, the seamount has a slope of  $14.04^\circ$ , and its radius is 2.5 km. The flat bottom is 825 m deep, and the tip of the seamount is 625 m high. The modeling results

shown in Fig. 3 is for the case where the seamount is centered at  $X = 2.5$  km and  $Y = 0$  km. On the vertical slice across the tip, the solutions from all of the models have good agreements, as shown in Fig. 2b to 2d. This is because no horizontal refraction occurs on this vertical plane. Both the 3D models predict a shadow zone behind the seamount (see Fig. 2e and 2f), and produce nearly identical interference patterns with  $\pm 30^\circ$  in azimuth.

## 5. Summary

Three-dimensional parabolic-equation approximate models with the Split-step Fourier algorithm are presented for underwater sound propagation in this paper. Requirements of the model grid size for resolving a given arrival angle and a given angular resolution are derived. A re-sampling technique is proposed for adjusting the model grids of a 3D cylindrical PE, and leads to a non-degraded model resolution, which a conventional cylindrical model usually suffers from. Examples of idealized slope and seamount are briefed, and the detailed model comparisons and further analysis of errors related to the grid sizes of environmental models will be presented in the talk.

## REFERENCES

- [1] F. D. Tappert, *Wave Propagation and Underwater Acoustics*, J. B. Keller and J. S. Papadakis, Springer-Verlag, pp. 224–287, 1977.
- [2] M.D. Feit and J.A. Fleck, Jr., “Light propagation in graded-index fibers,” *Appl. Opt.*, **17**, pp. 3990-3998, 1978.
- [3] D. J. Thomson and N. R. Chapman, “A wide-angle split-step algorithm for the parabolic equation,” *J. Acoust. Soc. Am.*, **74**, pp. 1848–1854, 1983.
- [4] L.-J. Huang, and M.C. Fehler, “Accuracy analysis of the split-step fourier propagator: implications for seismic modeling and migration,” *Bulletin of the Seismological Society of America*, **88(1)**, pp. 18-29, 1998.
- [5] T. F. Duda, *Initial results from a Cartesian three-dimensional parabolic equation acoustical propagation code*, Woods Hole Oceanographic Institution Tech. Rept., WHOI-2006-041, 2006.
- [6] F.B. Jensen, W.A. Kuperman, M.B. Porter, H. Schmidt, *Computational Ocean Acoustics*, R.T. Beyer, American Institute of Physics, pp. 375-379, 1994.
- [7] S.T. McDonald, “Propagation of normal mode in the parabolic approximation,” *J. Acoust. Soc. Am.*, **57**, pp. 307-311, 1975.
- [8] A.V. Oppenheim, R.W. Schaffer with J.R. Buck, *Discrete-Time Signal Processing*, A.V. Oppenheim, Prentice-Hall, Inc, pp. 172-176, 1989.

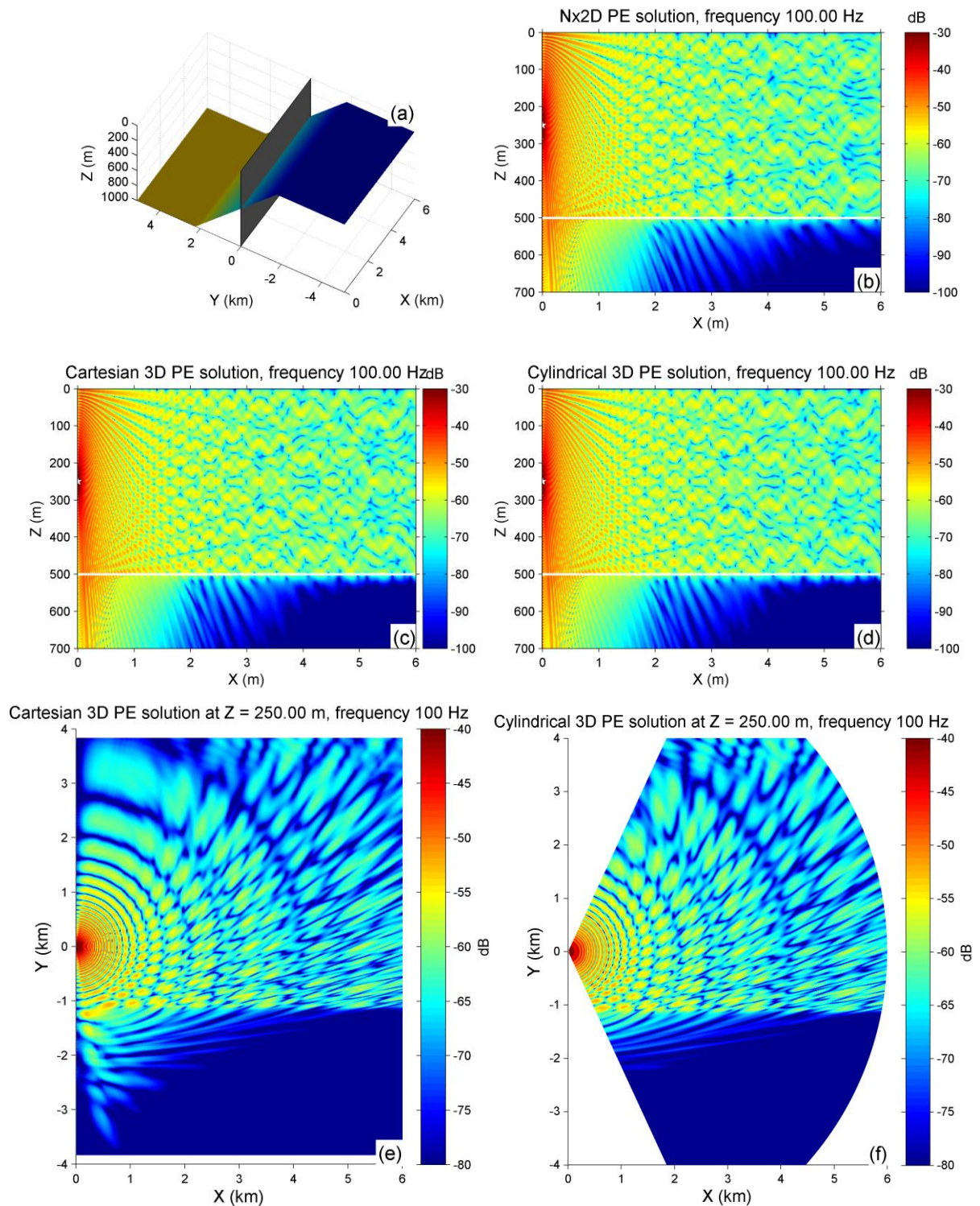


FIG. 2: 3D PE modeling results (100 Hz) for an idealized slope problem. Panel **a** is an illustration of the model considered. The vertical shaded slice shows the solution plane in panels **b** (Nx2D), **c** (Cartesian 3D) and **d** (cylindrical 3D with re-sampled azimuth grids). Panels **e** and **f** are comparisons of 3D PE solutions with employing different coordinate systems. The horizontal solution plane is at a constant depth 250 m across the computation domain.

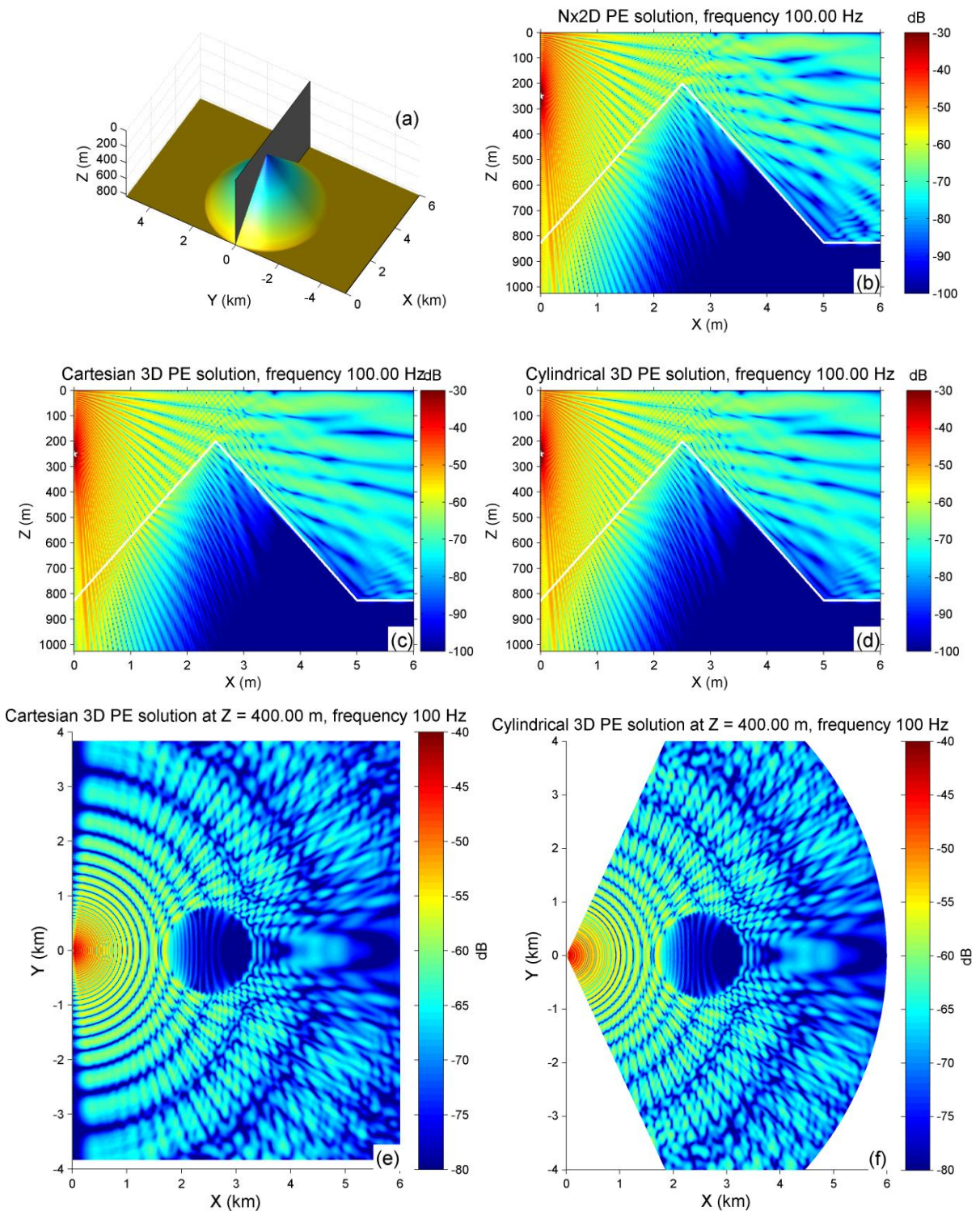


FIG. 3: 3D PE modeling results (100 Hz) for an idealized submarine seamount problem. Panel **a** is an illustration of the model considered. The vertical shaded slice shows the solution plane in panels **b** (Nx2D), **c** (Cartesian 3D) and **d** (cylindrical 3D with re-sampled azimuth grids). Panels **e** and **f** are comparisons of 3D PE solutions with employing different coordinate systems. The horizontal solution plane is at a constant depth 400 m across the computation domain.